Efficient Low-Voltage Ride-Through Nonlinear Backstepping Control Strategy for PMSG-Based Wind Turbine During the Grid Faults

M. Nasiri[1], J. Milimonfared[2], S. H. Fathi[2]*

[1]Department of Electrical Engineering, Faculty of Engineering, Abhar Branch Islamic Azad University, Abhar, Iran.
[2]Department of Electrical Engineering, Amirkabir University of Technology, Tehran 15875-4413, Iran.

Abstract-*This paper presents a new nonlinear backstepping controller for a direct-driven permanent magnet synchronous generator-based wind turbine, which is connected to the power system via back-to-back converters. The proposed controller deals with maximum power point tracking (MPPT) in normal condition and enhances the low-voltage ride-through (LVRT) capability in fault conditions. In this method, to improve LVRT capability, machine-side converter controls dc-link voltage and MPPT is performed by grid side converter. Hence, PMSG output power is reduced very fast and dc-link voltage variation is reduced. Due to nonlinear relationship between dc-link voltage and controller input, nonlinear backstepping controller has good performances. By applying the proposed controller, dc-link overvoltage is significantly decreased. The proposed controller has good performance in comparison with Proportional-Integral (PI) controller and Sliding Mode Controller (SMC). In asymmetrical faults, to decrease grid side active power oscillations, the nonlinear backstepping dual-current controller is designed for positive- and negative- sequence components. The simulation results confirm that the proposed controller is efficient in different conditions.*

Keyword: *Backstepping controller; Low voltage ride-through (LVRT); Maximum power point tracking (MPPT); Permanent magnet synchronous generator (PMSG); Wind turbine.*

NOMENCLATURE

Vectors and symbols

ρ	Specific density of air (kg/m^3)
A, r_{tur}	Blade swept area (m^2), Radius of blade (m)
β	Pitch angle ($^\circ$)
C_p	Power coefficient
v_w	Wind speed (m/s)
J_{eq}	Total equivalent inertia ($kg\,m^2$)
B_{eq}	Equivalent damping coefficient (Nms/rad)
p	Number of poles
ω_m	Mechanical shaft speed (rad/s)
R, L, C	Resistance (Ω),inductance (H)and dc-link capacitance (F)
V, i, ψ	Voltage (V),current (A) and flux (wb)
k	Positive gain
κ	Update gain
V	Grid side inverter voltage

subscripts

d, q	Direct and quadrature components
s	Stator of machine
f	Grid side
dc	dc-link

Superscripts

+,-	Positive and negative sequence
ref	reference

1. INTRODUCTION

Nowadays, the use of renewable energies has grown due to numerous advantages such as cleanness, accessibility and reliability [1]. Wind energy is one of the growing renewable energy sources of electricity at present [2]. According to the European wind energy association's 2020, wind power generation is satisfying 18.4% of European Union electricity demand [3]. Hence, the penetration level of wind power in the power system has considerably grown. Therefore, due to high penetration level of wind turbine systems, grid codes enforce wind turbines to remain connected to the grid in voltage drop conditions and inject the reactive current to the grid. The Fig. 1 shows the diagrams of requirements for tolerance of voltage drops and reactive current supply for wind turbines with capacity more than 1.5 MW in Danish grid code. This ability of wind turbines is well known as low-

voltage ride-through (LVRT) [4]. Although, there are different types of wind turbine, due to some advantages, Variable Speed Wind Turbine (VSWT) systems are attractive candidates on wind farms. Permanent magnet synchronous generators (PMSGs) are rapidly growing among VSWT systems. PMSG-based wind turbines offer some advantages, such as the gearbox elimination and increasing the reliability due to developments in semiconductor switching devices [5].

PMSG-based wind turbine is connected to the grid via back-to-back converters. When a fault occurs in the grid and the voltage deeply drops, the transferred power from dc-link to the grid is decreased. The generator, however, continues to generate electric power. Consequently, the dc-link voltage is highly increased. In such situation, the control of back-to-back converters might be lost and dc-link capacitor and switches are damaged [6].

Recently, several methods have been introduced to achieve LVRT capability of the PMSG that introduced in detail in [5]. The common LVRT solution is to connect braking chopper (BC) or active crowbar across dc-link capacitor terminals [7]. The advantage of this method is its low cost. However, it cannot improve the reactive power injection to the grid and dissipates active power. Therefore, energy storage systems (ESSs) are installed in the dc-link. ESSs perform power smoothing in normal condition and absorb additional energy in fault conditions, preventing the dc-link overvoltage [8, 9]. Although ESSs have fast response but their cost is high. FACTS devices are other options to improve LVRT capability in the wind turbines [10]. STATCOM and SVC are common FACTS devices that can inject reactive current to the grid [11, 12]. A Dynamic Voltage Restorer (DVR) is another device that compensates voltage sags [13, 14]. One of the main disadvantages of FACTS devices is their high cost. Another device to implement LVRT is series dynamic breaking resistor (SDBR). The SDBR is a series connected resistor between wind turbine and grid that it is brought to the circuit in fault conditions [5]. The main drawback of SDBR is lack of reactive current injection to the grid.

Finally, modified back-to-back converter controller is attractive method to improve LVRT capability due to low cost and efficient performance. In many papers, grid side converter (GSC) controls dc-link voltage [7-9]. In this case, generator continues to generate power and cannot sense grid side faults. Hence, Anca D. Hansen et al. [15] introduce a new control structure, in which machine side converter (MSC) controls the dc-link voltage and GSC controls the transferred power. The

mentioned control strategy in [15] is used in some papers such as [16-19]. In [16-17], LVRT capability is implemented by proportional-integral (PI) controller. PI controller has not good performances in nonlinear systems and depends on operating point. Although, in [18], in order to encounter the nonlinearity of the system, the MSC controllers is designed based on fuzzy logic. However, the GSC controller is based on PI controller and it has not good performances in asymmetrical grid faults. In [19], Due to nonlinearity in relation between dc-link voltage and mechanical speed, an input-output feedback linearization has been applied to the dc-link voltage control. In [20-21], sliding mode control (SMC) is applied to back-to-back converter controllers. In [21], chattering is the main drawback of designed controller, and the disadvantages of introduced controller in [20] are the using of PI controller in GSC and undesirable performance in asymmetrical grid faults.
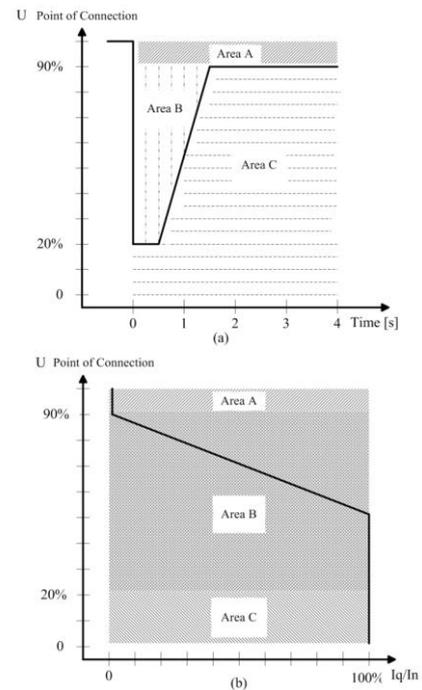
Fig. 1. The diagrams of requirements for (a) tolerance of voltage drops and (b) reactive current supply, for wind turbines with capacity more than 1.5 MW in Danish grid code [5].

Backstepping is one of the nonlinear control methods, which is employed for speed control in permanent magnet synchronous motors [22]. This controller, unlike sliding mode control [21], has chattering free feature. Hence, it is a proper choice for PMSG-based wind system applications. In [23], a backstepping control scheme for the back-to-back converter of PMSG-based wind turbines is designed. The MSC regulates the velocity of the PMSG with MPPT and the GSC controls the dc-link voltage and the reactive power flow, independently. Hence, the control scheme of [23], not only needs to

external devices to suppress the dc-link overvoltage and cannot inject reactive current to the grid according to new grid codes, but also it has not good performances in asymmetrical grid voltage sags because it controls positive sequence component.

This paper proposes a new nonlinear backstepping controller for back-to-back converter for LVRT capability enhancement in PMSG-based wind turbines in which, unlike the previous approaches, there is no need to additional devices. The GSC controller does MPPT and injects reactive current to the grid according to new grid codes. In fact, GSC acts as a STATCOM in fault conditions. In addition, the MSC controls dc-link voltage that it has good performance in the fault conditions. Furthermore, the proposed controller improves LVRT capability during deep symmetrical and asymmetrical grid voltage sags. In asymmetrical faults, to decrease grid-side active power oscillations, the nonlinear backstepping dual-current controller is designed for positive and negative sequence components.

As new contributions to earlier studies, the following subjects can be mentioned:

- First, a new nonlinear backstepping controller is designed for back-to-back converter;

- Second, the tasks of back-to-back converter controllers are exchanged, so that the GSC controller does MPPT and the MSC controls dc-link voltage;

- Third, the GSC controller is composed of both positive and negative sequence components of the current controllers, which provides the opportunity for reduction of grid-side active power oscillations in asymmetrical grid faults.

- Fourth, due to power loss in back-to-back converter and connecting wires, the accurate power measurement is difficult. Hence, in this work, the power loss estimation is used.

Using this approach, unlike [19], there is no need for PI controllers; as a result, the performance of dc-link voltage controller is improved; also, it does not depend on the operating point. Moreover, under the same conditions, the proposed controller is compared with the improved PI controller and sliding mode controller [21]. All taken together, provides a cost-effective technique in terms of implementation and maintenance.

The paper is organized as follows: Section 2 presents PMSG-based wind turbine model; Section 3 discusses the proposed LVRT controllers; Section 4 illustrates simulation results and comparison of the proposed

nonlinear backstepping with sliding mode and PI controllers. Finally, conclusions are made in section 5.

2. PMSG-BASED WIND TURBINE MODEL

2.1. Wind turbine model
Figure 2 shows the schematic diagram of the grid-connected PMSG-based wind turbine. Mechanical output power of the wind turbine is expressed by the following equation [24]:

$$P_{Tur} = 0.5\rho A C_p(\lambda, \beta) v_w^3 \tag{1}$$

where $C_p(\lambda,\beta)$ is defined by the following equations:

$$C_p(\lambda, \beta) = 0.5176(\frac{116}{\lambda_i} - 0.4\beta - 5)\exp^{(-\frac{21}{\lambda_i})} + 0.0068\lambda \tag{2}$$

$$\frac{1}{\lambda_i} = \frac{1}{\lambda + 0.08\beta} - \frac{0.035}{\beta^3 + 1} \tag{3}$$

And the tip-speed ratio (λ) depends on ω_m and v_w as given below:

$$\lambda = R\omega_m / v_w \tag{4}$$

The power equation of the system is expressed as:
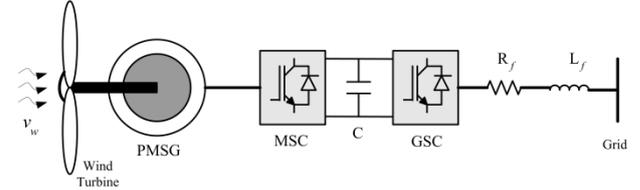
Fig. 2. The schematic diagram of the grid-connected PMSG-based wind turbine.

$$P_{Tur} = J_{eq}\frac{d\omega_m}{dt}\omega_m + B_{eq}\omega_m^2 + P_{gen} \tag{5}$$

2.2. Modeling of PMSG and dc-link

The state equations of a surface-mounted PMSG are expressed in the synchronous d-q coordinates as [16]:

$$L_s\frac{di_{ds}}{dt} = -R_s i_{ds} + \frac{p}{2}\omega_m L_s i_{qs} + V_{ds} \tag{6}$$

$$L_s\frac{di_{qs}}{dt} = -R_s i_{qs} - \frac{p}{2}\omega_m L_s i_{ds} - \frac{p}{2}\omega_m\psi + V_{qs} \tag{7}$$

The generator power is given as:

$$P_{gen} = \frac{3}{2}\frac{p}{2}\psi i_{qs}\omega_m \tag{8}$$

The state equation of the dc-link can be expressed as:

$$\frac{C}{2}\frac{d(V_{dc}^2)}{dt} = (P_{gen} - P_{loss} - P_{grid}) \tag{9}$$

Where P_{loss} is PMSG and back-to-back converter losses.

2.3. Interface reactor state equations

The wind system is connected to the grid via an interface reactor which serves as a low pass filter. The state equations of the filter in *d-q* frame can be expressed by:

$$L_f \frac{di_{df}}{dt} = -R_f i_{df} + \omega_f L_f i_{qf} + v_{df} - V_{df} \tag{10}$$

$$L_f \frac{di_{qf}}{dt} = -R_f i_{qf} - \omega_f L_f i_{df} + v_{qf} - V_{qf} \tag{11}$$

In unbalanced grid fault conditions, the positive and negative sequence components in d and q axes are expressed as:

$$L_f \frac{di_{df}^+}{dt} = -R_f i_{df}^+ + \omega_f L_f i_{qf}^+ + v_{df}^+ - V_{df}^+ \tag{12}$$

$$L_f \frac{di_{df}^-}{dt} = -R_f i_{df}^- - \omega_f L_f i_{qf}^- + v_{df}^- - V_{df}^- \tag{13}$$

$$L_f \frac{di_{qf}^+}{dt} = -R_f i_{qf}^+ - \omega_f L_f i_{df}^+ + v_{qf}^+ - V_{qf}^+ \tag{14}$$

$$L_f \frac{di_{qf}^-}{dt} = -R_f i_{qf}^- + \omega_f L_f i_{df}^- + v_{qf}^- - V_{qf}^- \tag{15}$$

Due to presence the negative sequence voltage and current components in asymmetrical grid faults, the active power is expressed as [25]:

$$p_{grid}(t) = P_0 + P_{c2}\cos(2\omega_f t) + P_{s2}\sin(2\omega_f t) \tag{16}$$

Where P_0 is average of active power, P_{c2} and P_{s2} are amplitude of second order components of active power.

The positive and negative sequence components of the current reference are obtained by controlling P_{c2} and P_{s2} to zero. The details of calculating current references can be founded in [19].

3. DESCRIPTION OF PROPOSED LVRT CONTROL

In this section, for convenience, the parametric transformations of the mathematical model of PMSG-based wind turbine, given in Eqs. (6)-(9) and (12)-(15), are rewritten as the followings:

$$a_{s2} \frac{di_{ds}}{dt} = -a_{s1}i_{ds} + \frac{p}{2}a_{s4}i_{qs} + V_{ds} \tag{17}$$

$$a_{s2} \frac{di_{qs}}{dt} = -a_{s1}i_{qs} - \frac{p}{2}a_{s4}i_{ds} - \frac{p}{2}a_{s3} + V_{qs} \tag{18}$$

$$\frac{1}{p}b_{s1}\frac{d(x_{dc})}{dt} = -i_{qs} - \frac{1}{p}b_{s2} \tag{19}$$

$$a_{f1}\frac{di_{df}^+}{dt} = -a_{f2}i_{df}^+ + a_{f3}i_{qf}^+ + v_{df}^+ - V_{df}^+ \tag{20}$$

$$a_{f1}\frac{di_{df}^-}{dt} = -a_{f2}i_{df}^- - a_{f3}i_{qf}^- + v_{df}^- - V_{df}^- \tag{21}$$

$$a_{f1}\frac{di_{qf}^+}{dt} = -a_{f2}i_{qf}^+ - a_{f3}i_{df}^+ + v_{qf}^+ - V_{qf}^+ \tag{22}$$

$$a_{f1}\frac{di_{qf}^-}{dt} = -a_{f2}i_{qf}^- + a_{f3}i_{df}^- + v_{qf}^- - V_{qf}^- \tag{23}$$

Where

$$a_{s1} = R_s, \; a_{s2} = L_s, \; a_{s3} = \psi\omega_m, \; a_{s4} = L_s\omega_m,$$
$$a_{f1} = L_f, \; a_{f2} = R_f, \; a_{f3} = L_f\omega_f,$$
$$b_{s1} = \frac{4C}{3\psi\omega_m}, \; b_{s2} = \frac{4(P_{loss} + P_{grid})}{3\psi\omega_m}.$$

To design MSC and GSC controllers, it is assumed that the state variables x_{dc}, i_{qs}, i_{ds}, i^+_{df}, i^-_{df}, i^+_{qf}, i^-_{qf} and the shaft speed signal (ω_m) are available.

3.1. Machine side converter controller

To design MSC controller, the dc-link voltage errors can be defined as:

$$e_{x_{dc}} = x_{dc} - x_{dc}^{ref} \tag{24}$$

In order to stabilize the dc-link voltage dynamics, the first positive definite Lyapunov function is expressed as follows:

$$z_1 = \frac{1}{2p}b_{s1}e_{x_{dc}}^2 \tag{25}$$

By taking time derivative of z_1, using Eqs. (19) and (24) and adding the term $\pm i_{qs}^{ref}$, the q-axis current reference can be defined as:

$$i_{qs}^{ref} = -\frac{1}{p}\hat{b}_{s2} - \frac{1}{p}b_{s1}\dot{x}_{dc}^{ref} + k_{s1}e_{x_{dc}} \tag{26}$$

Where k_{s1} is a positive constant and $\hat{b}_{s2}$ is b_{s2} the estimation. Due to power loss in back-to-back converter and connecting wires, the accurate power measurement is difficult. Hence, in this work, the b_{s2} estimation is used.

By defining $e_{qs} = i_{qs} - i_{qs}^{ref}$ and substituting (26) in time derivative of z_1, it follows that:

$$\dot{z}_1 = -e_{x_{dc}}e_{qs} - k_{s1}e_{x_{dc}}^2 - \frac{1}{p}\tilde{b}_{s2}e_{x_{dc}} \tag{27}$$

Where $\tilde{b}_{s2}$ is the estimation error of b_{s2}.

Now, backstepping can be applied on e_{qs} by defining the next positive definite Lyapunov function as follows:

$$z_2 = \frac{1}{2}a_{s2}e_{qs}^2 \tag{28}$$

By taking time derivative of z_2 and using (18), to stabilize q-axis current tracking dynamics, the q-axis control input can be defined as follows:

$$V_{qs} = a_{s1}i_{qs} + \frac{p}{2}a_{s4}i_{ds} + \frac{p}{2}a_{s3} + a_{s2}\dot{i}_{qs}^{ref} - k_{s2}e_{qs} + e_{x_{dc}} \tag{29}$$

By substituting Eq. (29) in the time derivative of z_2, it follows that:

$$\dot{z}_2 = e_{x_{dc}}e_{qs} - k_{s2}e_{qs}^2 \tag{30}$$

At this step, the third positive definite Lyapunov function is defined for d-axis current as follows:

$$z_3 = \frac{1}{2}a_{s2}e_{ds}^2 \tag{31}$$

By taking time derivative of z_3 and using Eq. (17), to stabilize d-axis current tracking dynamics, the d-axis control input can be defined:

$$V_{ds} = a_{s1}i_{ds} - \frac{p}{2}a_{s4}i_{qs} + a_{s2}\dot{i}_{ds}^{ref} - k_{s3}e_{qs} \tag{32}$$

The d-axis current reference is set to zero to reduce the copper loss. By substituting Eq. (32) in the time derivative of z_3, it follows that:

$$\dot{z}_3 = -k_{s3}e_{ds}^2 \tag{33}$$

At the last step of MSC controller design, positive definite Lyapunov function is defined to determine b_{s2} adaptation law and stability of the MSC controller. The Lyapunov function is expressed as follows:

$$z = z_1 + z_2 + z_3 + \frac{1}{2\kappa}\tilde{b}_{s2}^2 \tag{34}$$

By taking the time derivative of Eq. (34) and inserting Eqs. (28), (30) and (33) into the resulting equation:

$$\begin{aligned}\dot{z} = &-e_{x_{dc}}e_{qs} - k_{s1}e_{x_{dc}}^2 + e_{x_{dc}}e_{qs} - k_{s2}e_{qs}^2 \\ &-k_{s3}e_{ds}^2 + \tilde{b}_{s2}(-\frac{1}{p}e_{x_{dc}} + \frac{1}{\kappa}\dot{\tilde{b}}_{s2})\end{aligned} \tag{35}$$

To ensure asymptotic stability of the overall control system, the time derivative of the Lyapunov function should be non-positive. Hence, the updated law can be expressed as follows:

$$\dot{\tilde{b}}_{s2} = \kappa\frac{1}{p}e_{x_{dc}} \tag{36}$$

By substituting the updated law in (35) results in:

$$\dot{z} = -k_{s1}e_{x_{dc}}^2 - k_{s2}e_{qs}^2 - k_{s3}e_{ds}^2 \leq 0 \tag{37}$$

3.2. Grid side converter controller

In this paper, MPPT and generator output power smoothing are implemented by optimal power control (OPC) in the GSC. Hence, to extract maximum power from the wind turbine, the grid power reference is given by:

$$P_{grid}^{ref} = K_{opt}\omega_m^3 - B_{eq}\omega_m^2 - 1.5R_s(i_{ds}^2 + i_{qs}^2) \tag{38}$$

Where $K_{opt} = 0.5\rho A C_{p-\max}(r_{tur}/\lambda_{opt})^3$.

Asymmetrical grid faults are the most common in power system. To reduce harmful effects of these faults, dual current controller for positive and negative sequence components of grid current are used in the proposed method. By using dual current controller, fluctuation in injected active power to the grid is reduced. Also, MPPT is implemented in normal condition.

The grid voltage is oriented on d-axis. Hence, the q-axis voltage will be zero in normal condition.

To design positive and negative sequence components of d and q axes controllers, four positive definite Lyapunov functions are defined as follows:

$$z_4 = \frac{1}{2}a_{f1}e_{df}^{+\,2} \tag{39}$$

$$z_5 = \frac{1}{2}a_{f1}e_{df}^{-\,2} \tag{40}$$

$$z_6 = \frac{1}{2}a_{f1}e_{qf}^{+\,2} \tag{41}$$

$$z_7 = \frac{1}{2}a_{f1}e_{qf}^{-\,2} \tag{42}$$

To avoid repeating the procedure, control inputs of d and q axes are written as follows:

$$v_{df}^+ = a_{f1}\dot{i}_{df}^{+ref} + a_{f2}i_{df}^+ - a_{f3}i_{qf}^+ + V_{df}^+ - k_{f1}^+e_{df}^+ \tag{43}$$

$$v_{df}^- = a_{f1}\dot{i}_{df}^{-ref} + a_{f2}i_{df}^- + a_{f3}i_{qf}^- + V_{df}^- - k_{f1}^-e_{df}^- \tag{44}$$

$$v_{qf}^+ = a_{f1}\dot{i}_{qf}^{+ref} + a_{f2}i_{qf}^+ + a_{f3}i_{df}^+ + V_{qf}^+ - k_{f2}^+e_{qf}^+ \tag{45}$$

$$v_{qf}^- = a_{f1}\dot{i}_{qf}^{-ref} + a_{f2}i_{qf}^- - a_{f3}i_{df}^- + V_{qf}^- - k_{f2}^-e_{qf}^- \tag{46}$$

By substituting Eqs. (43) - (46) in to Eqs. (39) - (42), respectively, the asymptotic stability of the overall

control system is ensured.

4. SIMULATION RESULTS

To evaluate performances of the proposed nonlinear backstepping controller in direct-driven PMSG-based wind turbines, a simulation study has been carried out by MATLAB/Simulink software. Hence, the characteristics of a 1.5 MW PMSG-based wind turbine and parameters of the grid are given in Appendix A. Results of the proposed controller are compared with the results of a PI controller and sliding mode controller. The sliding mode controller of back-to-back converter is introduced in detail in [21]. Fig. 3 shows the PI controller of machine-side converter.
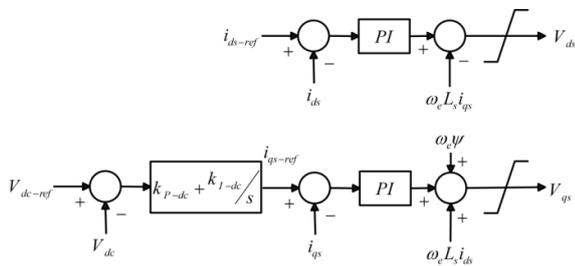
Fig. 3. The block diagram of the PI controller of machine-side converter.

In order to obtain the optimum parameters of PI controller, a 3φ symmetrical voltage sag is applied at the PCC. This fault causes voltage reduction in the grid voltage from 570 V to 200 V and last for one second, as shown in Fig. 4. Also, the wind speed is assumed 9 m/s.
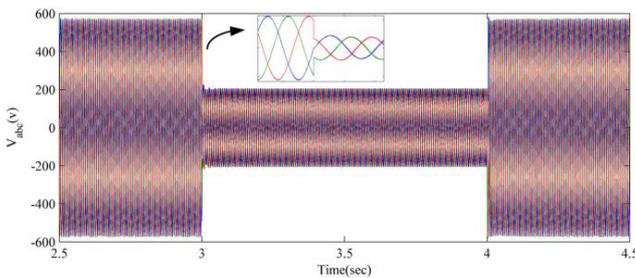
Fig. 4. Grid voltage in a 3φ symmetrical fault condition.

Figure 5 shows the percentage of maximum dc-link voltage overshoot with $k_{p\text{-}dc}$ and $k_{I\text{-}dc}$ variations. It can be seen that the system will be unstable by increasing kp_{-dc} and $k_{I\text{-}dc}$ larger than 3.5 and 35 respectively. It is worth noting that parameters of the PI controller are primarily adopted based on the Ziegler-Nicols method, and then optimally tuned through sensitivity of the dc-link voltage overshoot, as shown in Fig. 5.
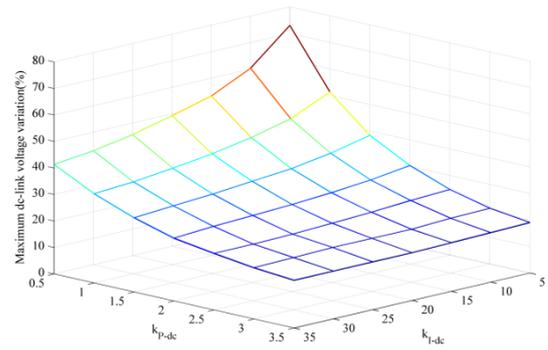
Fig. 5. The percentage of maximum dc-link voltage overshoot with $k_{p\text{-}dc}$ and $k_{I\text{-}dc}$ variations.

Figure 6 shows the dc-link voltage for different $k_{p\text{-}dc}$ s. Hence, to guarantee the stability of the closed-loop control system, $k_{p\text{-}dc}$ and $k_{I\text{-}dc}$ are set to 2.5 and 25, respectively.
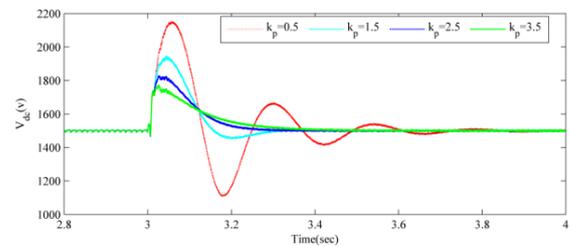
Fig. 6. The dc-link voltage waveform with different $k_{p\text{-}dc}$.

Figures 7 and 8 show block diagrams of MSC and GSC, respectively.
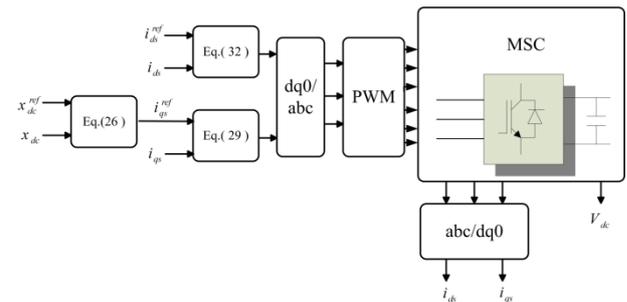
Fig. 7. Block diagram of the MSC controller.
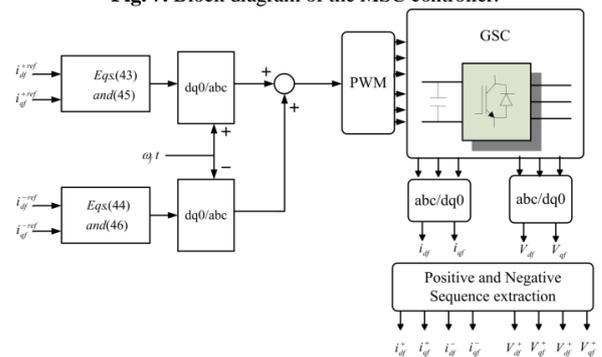
Fig. 8. Block diagram of the GSC controller.

Figure 9 shows the system performance in the normal condition. The wind speed is shown in Fig. 9 (a). The turbine and generator output power are shown in Fig. 9 (b). By using optimal power control method [24], the generator output power is smoothly changed by wind speed variations. The wind turbine speed, turbine power coefficient, pitch angle and dc-link voltage are shown from Fig. 9 (c)-(f). It can be seen that the controller has kept the dc-link voltage at the fixed reference. The turbine power coefficient is kept near 0.48; indicating satisfactory performance of the MPPT controller in GSC.

Figure 10 shows the performance of the system in estimating the parameter b_{s2}. The estimated b_{s2} is similar to the calculated b_{s2}.

To evaluate the performance of the controller in grid fault condition, it is assumed that a 3φ symmetrical voltage drop is occurred at the PCC, in accordance with Fig. 11 (a). The wind speed is set to 9 m/s. Fig.11 (b) shows the simulated dc-link voltage with the proposed controller compared with sliding mode and PI controllers. As it is observed in the Fig.11 (b), there is a large overshoot more than 25% of nominal value in the dc-link voltage with improved PI controller, which may cause the dc-link capacitor to fail. On the other hand, by using sliding mode controller, dc-link overvoltage is about 20% of nominal voltage. Furthermore, chattering
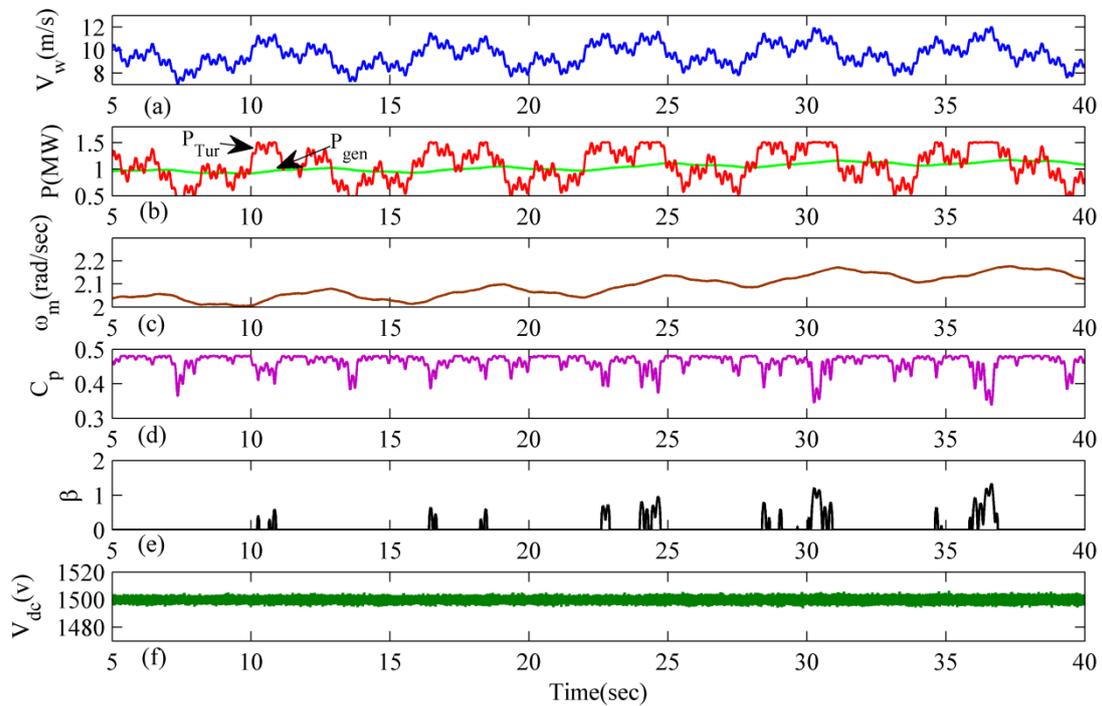
Fig. 9. Wind speed, generator output power, wind turbine speed, turbine power coefficient, pitch angle, and dc-link voltage in normal condition.
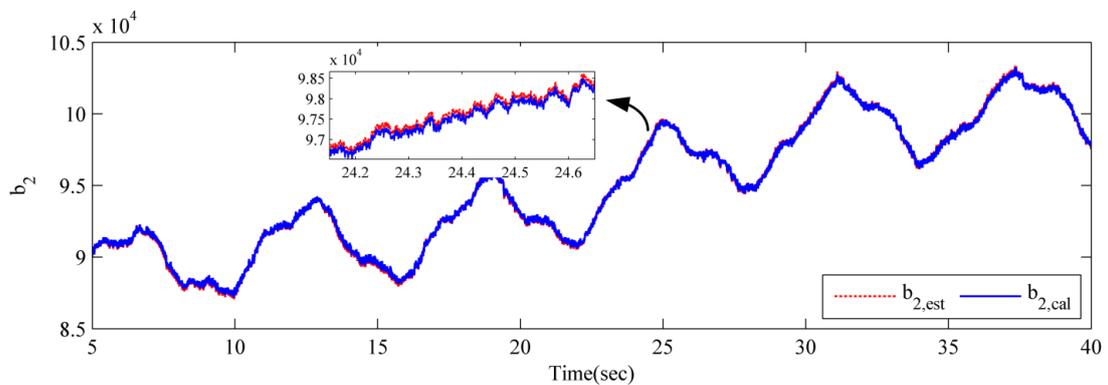
Fig. 10. Calculated and estimated b_{s2}.

in dc-link voltage is the main drawback of SMC. With the proposed nonlinear backstepping controller, however, the dc-link overvoltage is small and within the safety limit. At the fault inception, generator speed is rapidly raised with the proposed controller in comparison with sliding mode and PI controllers, as shown in Fig. 11 (c). This is the main reason of lower dc-link voltage overshoot with the proposed controller. In fact, the excess energy is stored as kinetic energy in total mass. Small changes in generator speed can cause a significant difference in dc-link voltage.

Figure 12 (a) shows the incoming active power to the PCC. As shown in Fig. 12 (a) active power is reduced

the amplitude of second-order harmonic fluctuations are decreased.
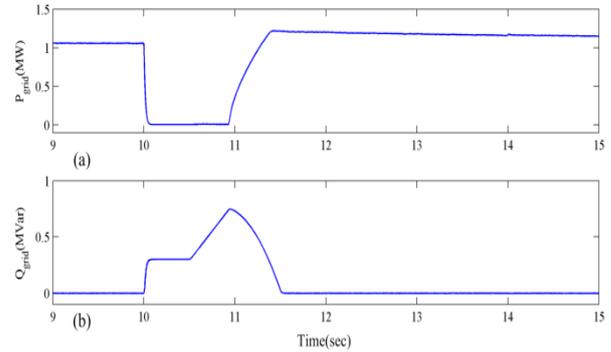
Fig. 12. (a) The injected active power to the grid, and (b) The injected reactive power to the grid during a 3φ symmetrical voltage drop in the
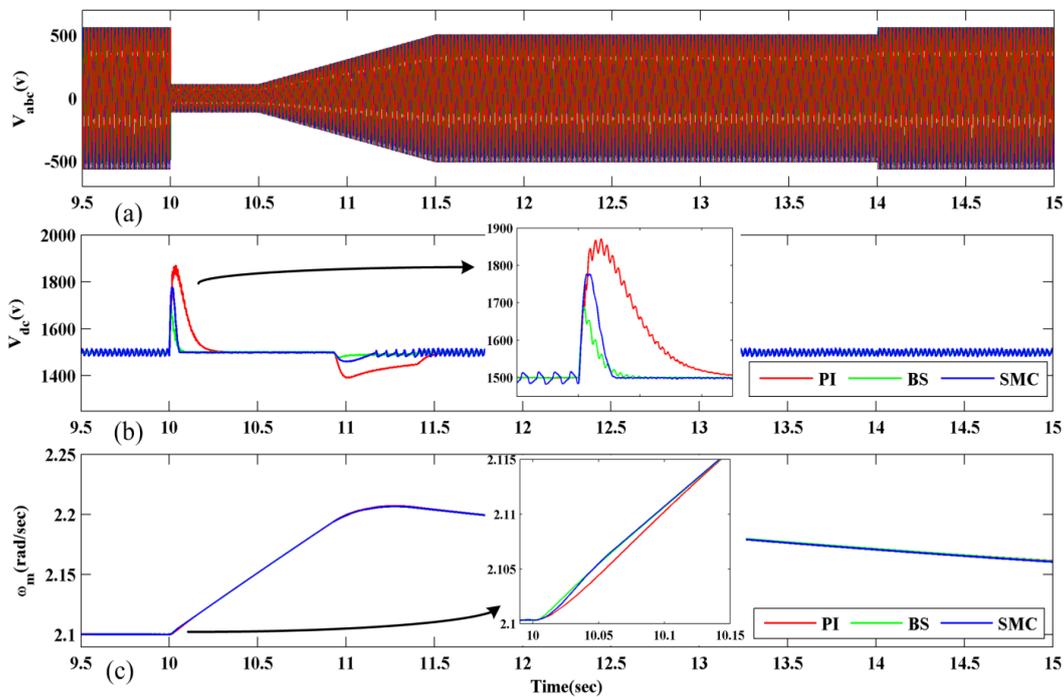
Fig. 11. (a) Grid voltage profile during a 3φ symmetrical voltage drop, (b) The dc-link voltage, and (c) Generator speed.

immediately and reactive power can inject to the grid as shown in Fig. 12 (c) according grid code compliance for reactive power injection in fault condition. In fact, during the fault, GSC acts as a STATCOM and injects reactive power to the grid.

To study the system performances against asymmetrical grid faults; a simulation is performed for a single-phase fault condition. Fig. 13(a) shows the voltage profile of phase A of the PCC, in which the voltage of phase A has dropped according Fig. 1(a). The PCC voltage was transferred to d-q components, and their positive- and negative-sequences were separated as shown in Fig. 13(b). Finally, dc-link voltage is shown in Fig. 13(c). Because of using new backstepping controller and dual-current controller, the dc-link overvoltage and

PCC.
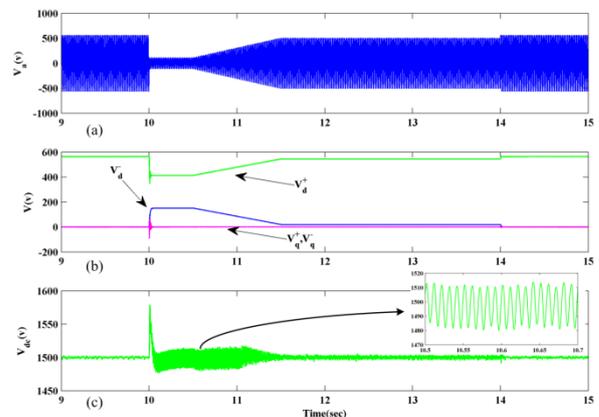
Fig. 13. (a) The voltage profile of phase A of the PCC, (b) PCC voltage in the synchronous d-q coordinates, and (c) dc-link voltage in 1φ voltage sag.

Figures 14 (a) and (b) present positive- and negative-sequence components of the GSC current for the proposed dual-current controller in the grid fault in accordance Fig. 13 (a), respectively. As shown in Fig. 14 (b), the negative-sequence is controlled in proposed controller. The injected current from GSC to the grid is shown in Fig. 14 (c). Because of using of dual-current controller, the current of all phases is kept in safe limit.

Figure 15 (a) implies that the proposed controller eliminates second-order component of active power (P_{s2-d} and P_{c2-d}). As a result, the second-order harmonic fluctuations of active power will be decreased (Fig. 15(b)). It is noteworthy here that proposed controller reduces the PMSG active power in the grid fault conditions. The injected reactive power to the grid is shown in Fig. 15(c).

5. CONCLUSIONS

This paper addresses a novel nonlinear backstepping controller for LVRT capability enhancement in PMSG-based wind turbine. The main advantages of the proposed method are; 1) there is no need to additional equipment, 2) it can meet the grid code requirements, 3) it is not dependent to the operating point, 4) it provides a simple and efficient technique. The proposed controller improves LVRT capability of PMSG during symmetrical and asymmetrical grid voltage sags. To reduce the undesired effects of asymmetrical faults, dual current controller for positive- and negative-sequence components of grid current are employed in the proposed method. Simulations in terms of robustness, effectiveness and LVRT capability, as well as the dc-link voltage regulation verified superiority of nonlinear backstepping controller over the conventional PI controller and sliding mode controller. Finally, using the proposed method, implementation and maintenance costs are efficiently reduced.
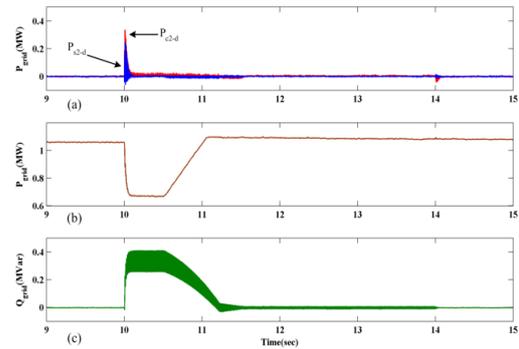
Fig. 15. (a) Second order components of active power positive sequence components, (b) The injected active power to the grid, and (c) The injected reactive power to the grid during 1φ fault condition.
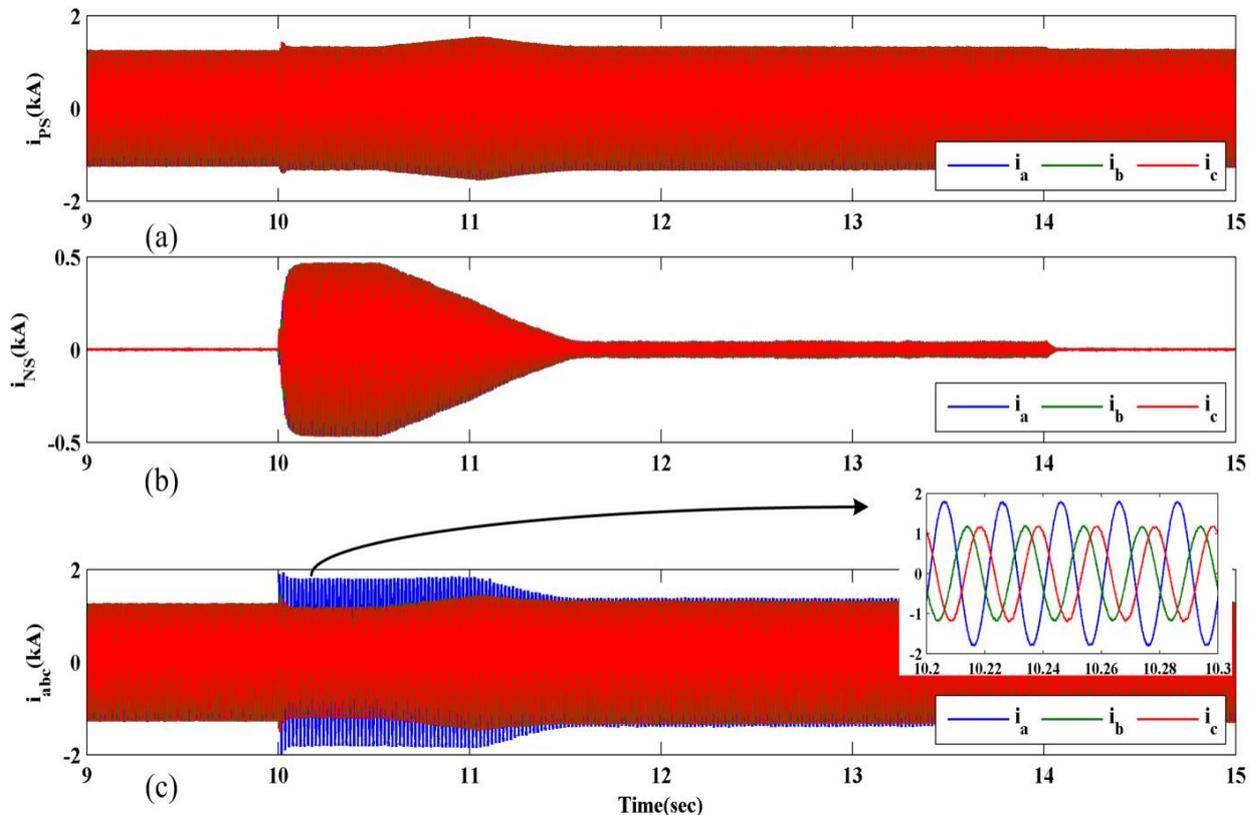
Fig. 14. (a) Positive sequence component, (b) negative sequence component of GSC current, (c) Injected current from GSC to the grid in 1φ

fault condition.

Appendix A.

Parameters of system:

Turbine) $R = 36.6\ m$, $\rho = 1.225\ kg / m^3$,

$J_{eq} = 4.87 \times 10^6\ kg.m^2$, $B_{eq} = 200\ N.m.s / rad$, $C_{p-\max} = 0.48$,

PMSG) 1.5 MW, 690 V. $R_s = 3.174\ m\Omega$, $L_s = 3.07\ mH$,

$\psi = 7.0172\ wb$, $p = 80$,

Back-to-Back converter) $C_{dc} = 0.023\ F$, $V_{dc} = 1500\ V$,

$f_{sw} = 10kHz$,

Grid) 690V, 50 Hz, $L_f = 0.44\ mH$.

REFERENCES

[1] A. Hatefi Einaddin, A. Sadeghi Yazdankhah and R. Kazemzadeh, "Power management in a utility connected micro-grid with multiple renewable energy sources," *J. Oper. Autom. Power Eng.,* vol. 5, no. 1, pp. 1-9, June 2017.

[2] H. Khorramdel, B. Khorramdel, M. Tayebi Khorrami and H. Rastegar, "A multi-objective economic load dispatch considering accessibility of wind power with here-and-now approach," *J. Oper. Autom. Power Eng.,* vol. 2, no. 1, pp. 60-73, 2014.

[3] EWEA, "EU Energy Policy to 2050 – Achieving 80-95% emissions reductions." http://www.ewea.org/publications/reports/eu-energy-policy-to-2050/.

[4] A. R. Nafar Sefiddashti and A. Elahi, "Low voltage ride through enhancement based on improved direct power control of dfig under unbalanced and harmonically distorted grid voltage," *J. Oper. Autom. Power Eng.*, vol. 4, no. 1, pp. 16-28, 2016.

[5] M. Nasiri, J. Milimonfared and S. H. Fathi, "A review of low-voltage ride-through enhancement methods for permanent magnet synchronous generator based wind turbines," *Renew Sustain. Energy Rev.*, vol. 47, pp. 399-415, July 2015.

[6] M. Nasiri, "A robust controller for permanent magnet synchronous generator based wind turbine in fault condition on the grid," Ph.D. dissertation, Dept. Elect. Eng., Amirkabir Univ. of Technology, Tehran, Iran, April 2015.

[7] T. H. Nguyen, D. C. Lee, "Advanced fault ride-through technique for PMSG wind turbine systems using line-side converter as STATCOM," *IEEE Trans. Ind. Electron.*, vol. 60, no. 7, pp. 2842-2850, 2013.

[8] Zh. Zhou, F. Scuiller, J. F. Charpentier, M. E. H. Benbouzid, and T. Tang, "Power smoothing control in a grid-connected marine current turbine system for compensating swell effect," *IEEE Trans. Sustain. Energy*, vol. 4, no. 3, pp. 816-826, Mar. 2013.

[9] R. Sarrias-Mena, L. M. Fernández-Ramírez, C. A. García-Vázquez, F. Jurado, "Improving grid integration of wind turbines by using secondary batteries," *Renew Sustain. Energy Rev.*, vol. 34, pp. 194-207, 2014.

[10] S. M. Muyeen, R. Takahashi, T. Murata, J. Tamura, "A variable speed wind turbine control strategy to meet wind farm grid code requirements," *IEEE Trans. Power Syst.,* vol. 25, no. 1, pp. 331-340, 2010.

[11] S. M. Muyeen, "A combined approach of using an SDBR and a STATCOM to enhance the stability of wind farm," *IEEE Syst. J.*, pp. 922-932, 2015.

[12] P. Kumar, N. Kumar, A. Akella, "A simulation based case study for control of DSTATCOM," *ISA Trans.*, vol. 53, pp.767-775, 2014.

[13] C. Wessels, F. Gebhardt, F. W. Fuchs, "Fault ride-through of DFIG wind turbine using a dynamic voltage restorer during symmetrical and asymmetrical grid faults," *IEEE Trans. Power Electron.*, vol. 26, no. 3, pp. 807-815, 2011.

[14] A. Y. Goharrizi, S. H. Hosseini, M. Sabahi, G. B. Gharehpetian, "Three-phase HFL-DVR with independently controlled phases," *IEEE Trans. Power Electron.*, vol. 27, no. 4, pp. 1706-1718, April 2012.

[15] A. D. Hansen, G. Michalke, "Modelling and control of variable-speed multi-pole permanent magnet synchronous generator wind turbine," *Wind Energy*, vol. 11, pp. 537-554, 2008.

[16] A. D. Hansen, G. Michalke, "Multi-pole permanent magnet synchronous generator wind turbines' grid support capability in uninterrupted operation during grid faults," *IET Renew. Power Gener.*, vol. 3, no. 3, pp. 333-348, 2009.

[17] J. Yao, L. Guo, T. Zhou, D. Xu, R. Liu, "Capacity configuration and coordinated operation of a hybrid wind farm with FSIG-based and PMSG-based wind farms during grid faults," *IEEE Trans. Energy Convers.*, vol. 32, Issue. 3, pp. 1188 - 1199, Sept. 2017.

[18] H. M. Yassin, H. H. Hanafy, M.M. Hallouda, "Low voltage ride-through technique for pmsg wind turbine systems using interval type-2 fuzzy logic control," Proce. *IEEE Int. Ind. Technol.*, pp. 1065-1070, 17-19 March 2015.

[19] K. H. Kim, Y. C. Jeung, D. C. Lee, H. G. Kim, "LVRT scheme of PMSG wind power systems based on feedback linearization," *IEEE Trans. Power Electron.*, vol. 27, no. 5, pp. 2376-2384, May 2012.

[20] D. Jeong, C. Kim, Y. Gui, C.C. Chung, "Sliding mode control for LVRT of a PMSG wind turbine using stored energy in rotor inertia," Proc. *Power Energy Soc. Gen. Meeting* , 17-21 July 2016.

[21] M. Nasiri, J. Milimonfared, S. H. Fathi, "Robust control of pmsg-based wind turbine under grid fault conditions," *Indian J. Sci. Technol.*, vol. 8, no. 13, July 2015.

[22] M. Karabacak, H. I. Eskikurt, "Design, modelling and simulation of a new nonlinear and full adaptive backstepping speed tracking controller for uncertain PMSM," *Appl. Math Model,* vol. 36, pp. 5199-5213, 2012.

[23] Y. Errami, A. Obbadi, S. Sahnoun, M. Benhmida, M. Ouassaid, M. Maaroufi, "Design of a nonlinear backstepping control strategy of grid interconnected wind power system based PMSG," Proce. *AIP Conf. Technol. Mater. Renewable Energy, Environ. Sustainability,* 1758, 030053-1–030053-13, July 2016.

[24] M. Nasiri, J. Milimonfared, S. H. Fathi, "Modeling, analysis and comparison of TSR and OTC methods for MPPT and power smoothing in permanent magnet synchronous generator-based wind turbines," *Energy Convers. Manage.* vol. 86, pp. 892-900, 2014.

[25] M. Nasiri, R. Mohammadi, "Peak current limitation for grid side inverter by limited active power in PMSG-based wind turbines during different grid faults," *IEEE Trans. Sustain. Energy*, vol. 8, no. 1, pp. 3-12, 2017.

[26] H. Geng, D. Xu, B. Wu, G. Yang, "Unified power control for PMSG based WECS Operating under different grid conditions," *IEEE Trans. Energy Convers.*, vol. 26, no. 3, pp. 822-830, Sep. 2011.